ACS NANO
Cite This: ACS Nano 2018, 12, 4529–4535
www.acsnano.org

ARTICLE

Enhancing the Strength of Graphene by a Denser Grain Boundary

Jie Xu,[†] Guowen Yuan,[†] Qi Zhu,[‡] Jiangwei Wang,[‡] Shan Tang,[§] and Libo Gao*[,†]

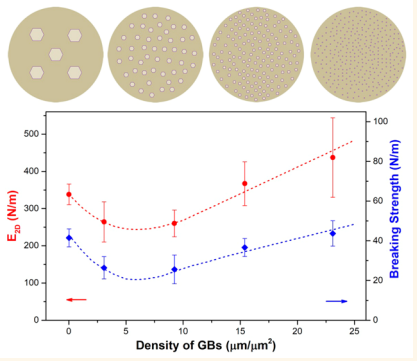
[†]National Laboratory of Solid State Microstructures, School of Physics, Collaborative Innovation Center of Advanced Microstructures, Nanjing University, Nanjing 210093, China

[‡]Center of Electron Microscopy and State Key Laboratory of Silicon Materials, School of Materials Science and Engineering, Zhejiang University, Hangzhou 310027, China

[§]Department of Mechanicals, Dalian University of Technology, Dalian 116024, China

Supporting Information

ABSTRACT: From a device application point of view, the extreme mechanical strength of graphene is highly desirable. However, the unavoidable polycrystalline nature of graphene films produced by chemical vapor deposition (CVD) leads to significant fluctuations in mechanical properties. Although the effects of atomic defects or grain boundaries (GBs) on mechanical strength have been widely studied and some modifications have been applied to enhance the stiffness of graphene, the problems of fragility as well as significantly reduced breaking strength arise. Here we report a systematic study on the effect of elastic modulus and breaking strength of CVD-derived graphene films with a controlled density and distribution of GBs. We find that graphene films become much stronger by hugely increasing the density of GBs without triple junctions (TJs) formed inside, in analogy to the two-dimensional (2D) plum pudding structures. The comprehensive performance with a 2D Young's modulus of 436 N/m (~1.3 TPa) and 2D breaking strength of 43 N/m (~128 GPa) can be achieved with the average grain size of 20 nm. Moreover, the existence of TJs will slightly reduce the strength in these GB structures. Due to defect types, the graphene films will show various tearing behaviors after indentation. All these mechanical studies of GBs provide a guideline to obtain the optimal performance of 2D materials through GB structure engineering.



KEYWORDS: *nanocrystalline graphene, grain boundary, AFM nanoindentation, mechanical properties, breaking strength*

With a Young's modulus of ~1 TPa (~340 N/m) and a breaking strength of ~125 GPa (~42 N/m), graphene is considered to be the strongest material,[1] applicable in future flexible electronics, wear-resistant coatings, and reinforcements in advanced composite materials. However, with its strong C−C sp^2 covalent bonds, graphene lacks plasticity. Atomic vacancies (point defects) and grain boundaries (GBs, plane defects) can easily change its mechanical strength.[2,3] The effects of point defects have been widely investigated through Ar ion irradiation,[4] O_2 plasma,[5] and high-energy He.[6] The large-scale vacancy regions caused by O_2 plasma significantly impair mechanical properties.[5] In contrast, the Young's modulus of graphene is reduced but remains nearly constant (0.8 TPa) even under high-energy He ion irradiation.[6] A higher Young's modulus of ~1.6 TPa (550 N/m) can be realized by introducing a controlled density of point defects by Ar ion irradiation,[4] along with a 30% reduction in breaking strength and confining crack propagation.[7] For plane defects, GBs inevitably exist in chemical vapor deposition (CVD)-derived graphene films.[3,8,9] Some theoretical studies suggest that GBs with highly tilted angles can achieve a near-intrinsic failure strength,[10] and experimental measurements also verified the approximately high elastic modulus across a single GB, along with a slight reduction of its breaking strength.[11] The statistical theory predicts the GB network will extensively affect the mechanical properties of polycrystalline graphene films when their average grain size is less than 25.6 nm.[12] Stress concentration tends to occur at the triple junctions (TJs) in these GB networks,[13] and the TJs can be considered to have a similar effect on mechanical properties to those of the point defects,[4] which will increase the elastic modulus but heavily reduce the breaking strength. Limited by the recent growth method, the average grain sizes of thermal CVD graphene films are always larger than 200 nm,[14] and the experimental mechanical properties for graphene films with nanocrystalline grain size remain unknown.

In this study, we grow graphene films with different grain sizes and GB structures by inductively coupled plasma CVD

Received: February 2, 2018
Accepted: April 16, 2018
Published: April 16, 2018

© 2018 American Chemical Society

DOI: 10.1021/acsnano.8b00869
ACS Nano 2018, 12, 4529–4535

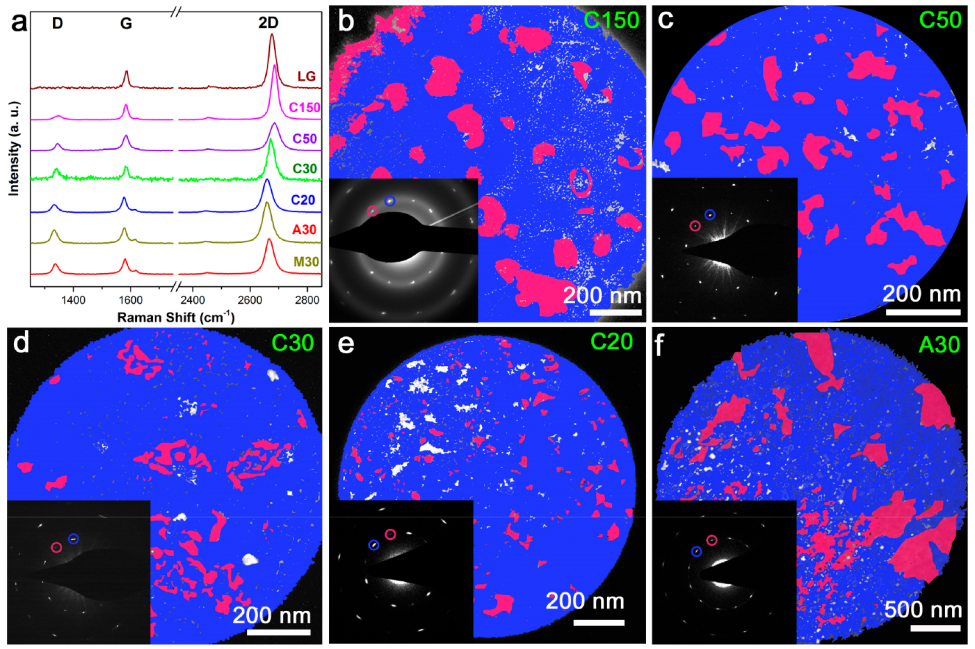


Figure 1. Plum pudding structured graphene films with different grain sizes. (a) Raman spectra of seven suspending graphene films used in this study, transferred on a hole-patterned SiO_2/Si substrate. (b–f) False-colored DF-TEM image of related C150, C50, C30, C20, and A30 films. The different colors represent the different grain orientations; insets are SAED patterns and selected areas are all 500–1000 nm.

(ICP-CVD) and thermal CVD methods, respectively. For growing highly flat graphene films, we adopt Cu/Ni alloy films as growth substrates. The single-crystalline Cu/Ni(111) and Cu/Ni(100) films are magnetron sputtered on the C-plane and A-plane sapphires (Supplementary Figure S1), and the polycrystalline Cu/Ni films are sputtered on the M-plane sapphire.[15] We use different faced metal films as substrates to grow individual graphene grains with different structures. Moreover, the grain sizes of graphene films have been tuned by changing growth temperature and plasma source power together, and higher temperature along with weaker plasma usually causes larger grain size (Supplementary Figure S2). Some growth results have been reported in our previous paper.[15] The graphene films with a grain size of >50 μm have been obtained by thermal CVD method. A traditional wet method has been performed using ammonium persulfate as etchant.[16] After transfer, we have characterized all the suspended graphene films on hole-patterned SiO_2/Si or transmission electron microscopy (TEM) grids by Raman spectroscopy (Figure 1a). Compared to the samples transferred on SiO_2/Si (Supplementary Figure S3), all these films have a similar intensity ratio of I_D to I_G, but higher intensities of the 2D band appear. Before the grains are completely stitched into a film, we can capture the individual grains by shortening the growth time and obtaining the average grain size. To normalize the graphene films from different growth conditions used in this study, we name them based on the growth substrate and their average grain size (nm) before stitching them into films: C150 (C-plane sapphire, average 150 nm grain size), C50, C30, C20, A30, M30, and large grain graphene (LG) with a grain size of >50 μm.

Generally, dark field transmission electron microscopy (DF-TEM) has been frequently applied to characterize the grain orientation in CVD graphene films,[3] and we also perform a similar DF-TEM with a large selected area electron diffraction (SAED) size of ~500 nm to characterize their GB structures. From the intensities of SAED, all the graphene films of the C series consist of grains with mainly two different orientations (insets of Figure 1b–e): one is in the majority (75–90%, oriented), and the other is in the proportion of 10–25% (anti-oriented). We also calculate the ratio of oriented to anti-oriented by region areas and find that they have similar results, shown in Supplementary Figure S4. The grains in A series films also have two main sets of diffraction patterns (inset of Figure 1f), but their intensities are comparable (>35% in anti-orientation), indicating roughly similar proportions in each orientated grain. These DF-TEM images (Figure 1b–e) are captured according to the SAED patterns, showing that a small quantity of anti-oriented grains is embedded in the combined C series film, without aggregation into larger anti-oriented grain regions. This GB structure in the homogeneous graphene films is similar to the plum pudding atomic model suggested by J. J. Thomson,[17] but in two dimension. In the A series film, the oriented and anti-oriented grains are interactively distributed, and some grains of the same orientation are stitched into large grains, indicating that a GB network is formed. Therefore, the TJs in the GB network should be massively formed in the A series, and this structure should be consistent with the proposed model of polycrystalline graphene films in these previous studies.[13,18] All the atomic lattices of the internal grains for all samples are defect-free (Supplementary Figure S5), such that the defects should only come from the GB structures.

AFM nanoindentation[1,19,20] has been used to measure the mechanical properties of 2D materials, and a schematic illustration is plotted in Figure 2a. AFM indentation displacements on the suspended graphene films are performed with a tip (13.9 nm radius) and a constant rate of 50 nm/s to acquire the force (F) *versus* indentation (d) curves, which can be approximated as[1]

DOI: 10.1021/acsnano.8b00869
ACS Nano 2018, 12, 4529–4535

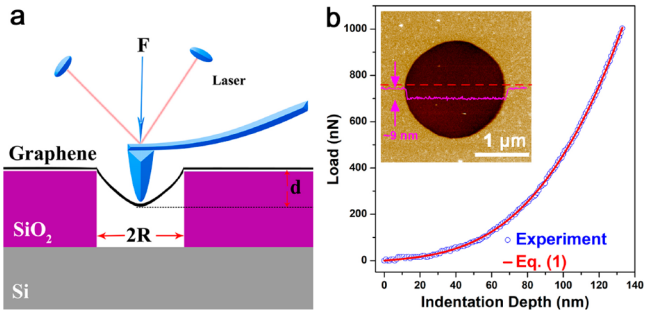


Figure 2. Mechanical measurement of suspended graphene films by AFM nanoindentation. (a) Illustration of the suspended graphene film on a hole-patterned SiO_2/Si wafer for AFM nanoindentation. (b) Typical force−displacement curve of LG films during AFM nanoindentation. The solid lines are fitting curves by eq 1, and the inset is a typical AFM image of the suspended graphene film before indentation test and the height profile along the red line showing the ~9 nm indentation in the hole.

$$F = \sigma_0^{2D}\pi d + E^{2D}q^3\frac{d^3}{R^2} \quad (1)$$

where σ_0^{2D} is the pretension accumulated in the membrane, E^{2D} is the elastic constant with units of force/length, R is the radii of the patterned hole (shown in Figure 2a), and q is a constant related to Poisson's ratio (ν) of the membrane, following $q = 1/(1.05 - 0.15\nu - 0.16\nu^2)$. We take $\nu = 0.165$, such that $q = 0.98$.[1] The elastic modulus of the films is $E^{3D} = E^{2D}/t$, where t is the thickness of films (0.335 nm for graphene). The pretensions for different films range from 0.05 to 0.4 N/m, with no correlation of the film types inside in spite of their different GB structures (also refer to Supplementary Figure S6).[4] The typical force−indentation curves of LG graphene films are plotted in Figure 2b, and the elastic stiffness of ~334 N/m can be obtained by fitting eq 1, which corresponds to ~997 GPa of E^{3D}. This value is not statistically different from that of previously obtained pristine[1] and CVD-grown graphene with large grains, no matter how much R is (Supplementary

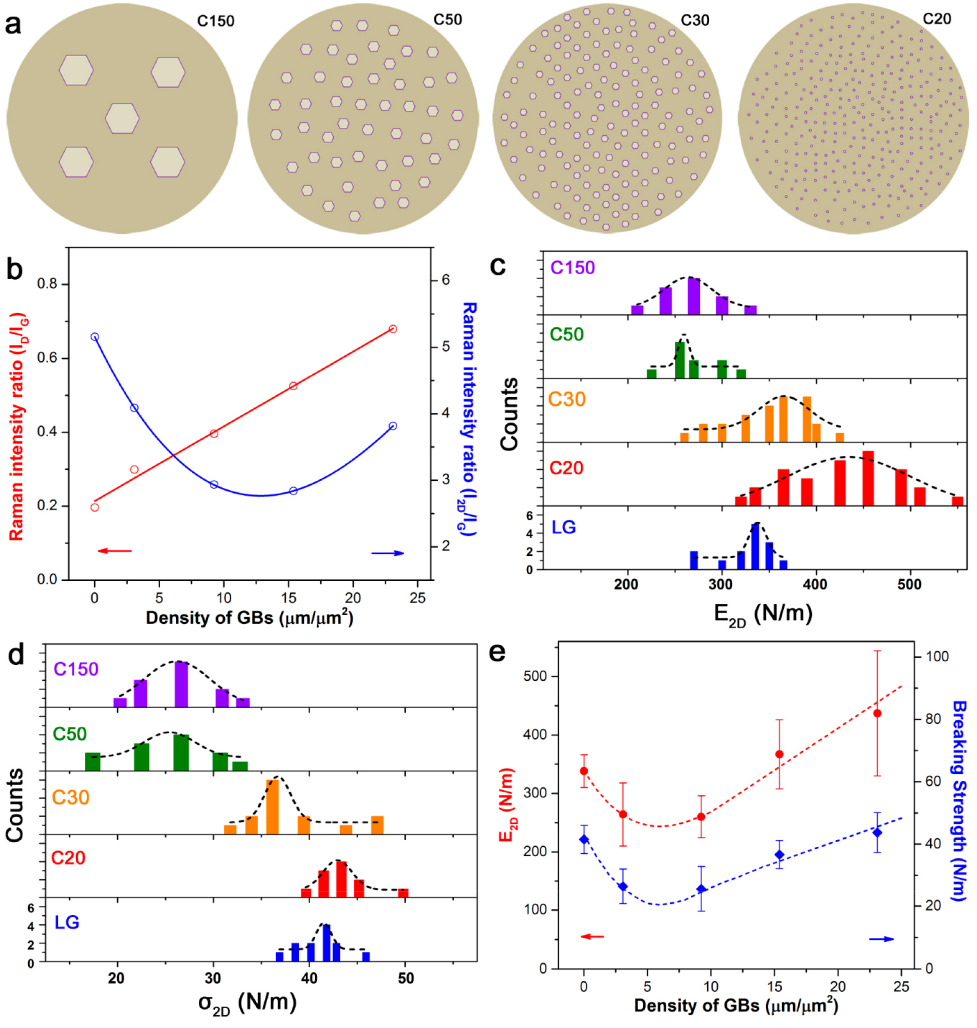


Figure 3. Mechanical properties of graphene films. (a) Illustration of C150, C50, C30, and C20 films, with plum pudding structure of different grain sizes; dark regions represent oriented grains, bright regions represent anti-oriented grains, and purple lines represent GBs. (b) Raman intensity ratio of I_D/I_G and I_{2D}/I_G as a function of GB density inside, showing the D bands (defect related) increase linearly with the GB density. (c) Histogram showing the comparison of elastic stiffness among graphene films with different grain sizes, along with LG films. (d) Histogram showing a comparison of breaking strengths, which are fitted with a nonlinear model. (e) Elastic modulus and breaking strength as a function of GB density inside; error bars correspond to the standard deviation of measurements performed on different graphene films, and dashed lines are fitted to the discrete results.

DOI: 10.1021/acsnano.8b00869
ACS Nano 2018, 12, 4529−4535

Figure S7).[19] In the measurement for LG films, we do not observe any correlation between the calculated pretension and E_{2D} (Supplementary Figure S6).[1,4,21] The breaking strength of these films could be acquired by measuring fracture loads and tip diameter with an experimentally validated multiscale model based on atomic-scale *ab initio* density functional theory, which gives a continuum description of anisotropic and nonlinear elastic behavior for in-plane deformation.[1,19] We also performed a linear model for the breaking strength by $\sigma = \sqrt{F_{max}E^{2D}/4\pi r_{tip}}$ for comparison, where F_{max} is the corresponding breaking force.[1,7] The breaking strength is obtained to be ~41.5 N/m (~124 GPa) and 46.6 N/m (~139 GPa) by nonlinear model and linear model, respectively. The linear model usually overestimates the strength about 10−20% compared with the nonlinear model,[1] while both models have been widely adopted and discussed in previous studies.[1,4,6,7,11,19] In the following discussion, we adopt the nonlinear model to fit the breaking strength.

RESULTS AND DISCUSSION

All C series of graphene films have the plum pudding structure and consist of mostly pure GBs with a few TJs inside. The effect of GB density on the mechanical properties can be well studied by these films. Illustrations of different GB distributions about the C series are shown in Figure 3a, according to the DF-TEM images in Figure 1b−e and their average size of individual grains before stitching into films.[15] These GBs exhibit hexagonal structures, and almost no networks are formed. Therefore, few TJs are formed in C series graphene films. The GB density is thus estimated to be $\rho \approx 0.46a^{-1}$ (Supplementary Figure S8), where a is the lateral size of the anti-oriented grains. The refined grains result in a larger GB area, which can also be verified by their Raman intensity ratios of different bands (Figure 3b). All the Raman spectra come from the suspended graphene films before nanoindentation measurements, and the Raman band intensities are collected by the area under the curves.[17,18] There should be only one type of main defect in these C series films, so the intensity ratios of I_D to I_G would indicate the presence of GBs, and they indeed present an approximately linear relation with our modeled density of GBs in Figure 3a. The ratio of I_{2D} to I_G first declines to a valley bottom at medium GB density, then slightly rises with increasing GB density, which is similar to the effect of vacancy-type defects by oxygen plasma radiation.[5] Moreover, there are no obvious changes in the Raman measurement before and after indentation (Supplementary Figure S9), indicating that the graphene films just show elastic transformation and have no structural destruction.

Figure 3c presents the statistical histogram of the elastic stiffness obtained from plenty of nanoindentation tests, with more than 10 collections for each sample. The average fitted 2D Young's modulus of 263, 259, 367, and 436 N/m for C150, C50, C30, and C20 films correspond to a bulk Young's modulus of 0.78, 0.77, 1.09, and 1.30 TPa, along with the 338 N/m (1.01 TPa) for LG films. Their breaking strengths are also plotted in Figure 3d statistically, and the average strengths of 26.4, 25.4, 36.6, and 43.1 N/m for the above films are obtained. The breaking strength of C20 films with higher GB density is comparable to that of an LG film (41.5 N/m), showing ~128 GPa when expressed as a 3D value. To better compare the breaking strength, we have also calculated the values by using linear and nonlinear models (Supplementary Figure S10). Although the calculated breaking strength values from the nonlinear model are a little lower than the one from the linear model, the changing rule for different densities of the GB is still quite clear. For better comprehension, we plot their elastic modulus and breaking strength as a function of GB density inside, as shown in Figure 3e. The dashed lines connecting the discrete results clearly reveal the trends. A small amount of GBs will reduce the mechanical properties, but it is amazing to find that their elastic and breaking strength rebound when further increasing the density of GBs. The refined grains bring in a higher GB density and the strength is enhanced. Therefore, the mechanical behavior would be enhanced by continuing to refine these grains. For fracture behavior, to our knowledge, refining grains should be the first promising approach to improve the breaking strength until now, even though the strength value is still about 10% lower than the intrinsic ones.[19] With higher GB density, these breaking strength values of C20 films (with the smallest grain size in this study) are not statistically different from previous large grain sized CVD-graphene films.

Until now, the theoretical calculations mostly predict that the stiffness and breaking strength of nanocrystalline graphene films with smaller grains will both be reduced,[22,23] but our experimental results show a completely different scenario. The discrepancy with theoretical results arises from the special GB structure in our specific graphene films with nanocrystalline grains. We find that, in the theoretically proposed GB models, there are plenty of TJs formed.[22,23] Similar to point defects, a low density of TJs can greatly increase the elastic modulus,[21] which is attributed to the local stress fields created by point defects. When the distance between two TJs is far enough, their interaction will not be very strong. If the TJs are closely connected, it will cause severe prestress concentration regions, which will induce cracks during elastic transformation.[12] In contrast, there are nearly no TJs formed in C series graphene films, and highly tilted GBs are composed of a series of prestrained pentagonal and heptagonal lattices.[23] These defects in GBs are isolated and scattered on the 2D plane, which are smaller compared with the proposed models in theoretical simulations. These small-sized defects from independent GBs will be analogous to the low density of point defects. As mentioned above, it can increase the Young's modulus. The more of these small defects, the more debonding energy will be dissipated between two grains during the fracture process. Finally, the breaking strength becomes comparable with that of pristine graphene. Therefore, the formation and distribution of these TJs are proposed to be a crucial factor in the mechanical performance of nanocrystalline graphene films.

For further analyzing the effects of TJ distribution, we grow graphene films with different densities of TJs. These graphene films are grown on different substrates, which leads to different grain structures, and the corresponding illustrations are plotted in Figure 4a. The grains in M series films have random orientations (see Supplementary Figure S11), and all the individual grains are finally stitched into humongous films. From the Raman spectra, there are larger GB regions and more TJs existing in A30 and M30 films, which is verified by stronger D and D′ bands (Supplementary Figure S3). From the same mechanical measurements, the statistical histograms of the stiffness and strength are plotted and shown in Figure 4b and c. The fitted 2D elastic modulus of average 248 and 300 N/m corresponds to a bulk Young's modulus of 0.74 and 0.89 TPa for M30 and A30 films, and their breaking strengths are ~32.5

DOI: 10.1021/acsnano.8b00869
ACS Nano 2018, 12, 4529−4535

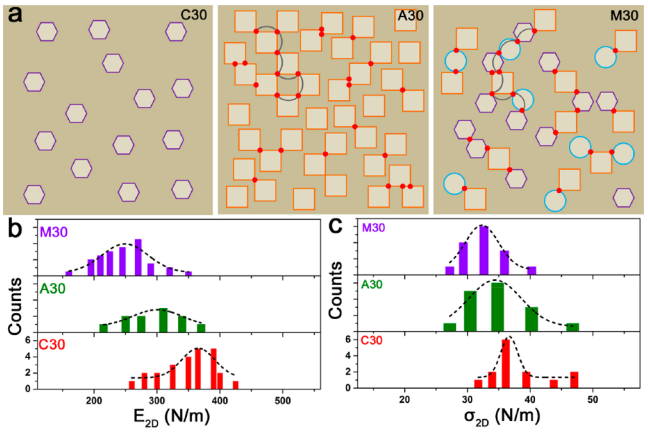


Figure 4. Mechanical properties of graphene films with different densities of TJs. (a) Illustration of C30, A30, and M30 graphene films with different densities of TJs; dark regions represent oriented grains, bright regions represent anti-oriented (purple hexagons and yellow squares) or disoriented (blue circles) grains, and red dots represent the sites of TJs. (b) Statistical histogram of elastic stiffness fitted from eq 1. (c) Statistical histogram of breaking strength based on the nonlinear model.

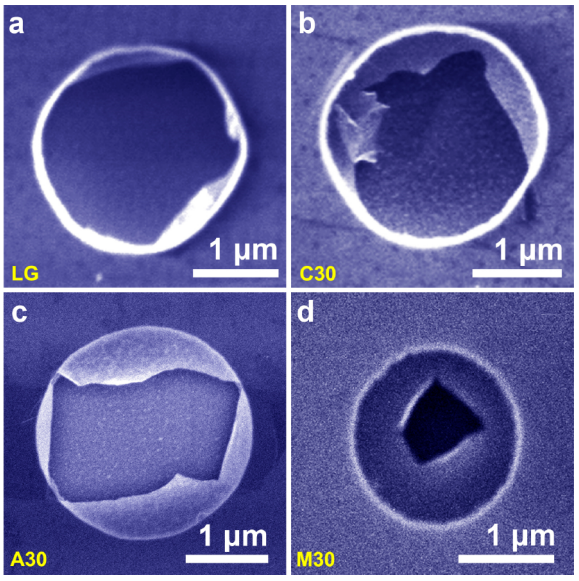


Figure 5. Tear performance of graphene films with different grain structures. SEM images of graphene drumheads acquired after fracture. The respective graphene films are LG (a), C30 (b), A30 (c), and M30 (d) films.

and ∼34.6 N/m. With highly disoriented and the misoriented grains stitched into a larger density of GB networks, the M30 films exhibit worse stiffness and breaking strength than those of A30, but A30 is worse than C30. Larger defect regions will be formed from the TJs (marked by black curves) of M30, A30, and C30 in order, illustrated in Figure 4a. This is consistent with our hypothesis and reported results that large defects caused by the TJs leads to a lower elastic modulus and breaking strength. Therefore, a high density of GB will enhance the strength, but a high density of TJs will reduce their strength.

The indenting tears and their propagation on the graphene films can also reveal their own GB structures due to the anisotropy of fracture behavior, just like bulk crystals.[24,25] Generally, fracture in polycrystalline graphene easily originates at a defect location and then propagates along the rest of the prestress regions.[3,12] When the LG and C30 films are broken, complete failure of the sheets proceeds rapidly across the whole well (Figure 5a and b),[19] and the tearing performance of the C30 film with few TJs is more like intrinsic graphene (LG).[1] The reason is that the plane defects are isolated and scattered evenly on the 2D plane, illustrated in Figure 4a, where the crack initiates. The tear of the A30 film exhibits a rectangle shape, and the crack propagates along the GB networks. M30 film with random tilted grains exhibits minor crack propagation in contrast to other films. Although different from the minor crack propagation in graphene films with point defects induced by Ar ion irradiation,[7] these M30 films still exhibit high stability against catastrophic failure and only a 28% decrease in elastic modulus. Therefore, the tear length is not only determined by the density of GBs but also strongly dependent on the distribution of GBs. The controlled defect creation will be an approach to confine crack propagation in polycrystalline graphene and further avoid catastrophic failure of graphene films in future devices.

CONCLUSIONS

In summary, we study the mechanical properties of graphene films with controlled grain size and different GB structures. Their mechanical performances show a strong dependence on the density of GBs and formed TJs. By engineering the GB distribution, we find the graphene films with a high density of GBs and few TJs possess better comprehensive mechanical properties, including the elastic modulus and breaking strength. When the average grain size is reduced to ∼20 nm, the effective Young's modulus of the corresponding graphene films could be larger than 1.3 TPa, along with a breaking strength higher than 128 GPa. Moreover, the tear propagation after indentation to fracture is also studied, and the nanocrystalline graphene films with disoriented grains exhibit a smaller tear region. All these studies could be a guideline to model the graphene GB structures for improved mechanical performance, and these structure−property relationships indicate a potential guideline for using graphene in flexible electronics and composite materials.

EXPERIMENTAL SECTION

CVD Growth of Graphene. The partially or fully covered graphene is grown in a customized ICP-CVD system. The typical growth conditions are as follow: sapphire with 800 nm sputtered Cu/Ni (20:1) film is heated to 700−850 °C at 6 Pa in an atmosphere of pure Ar. For the growth of graphene film, a mixture of H_2 and CH_4 (H_2/CH_4 = 20:1) is introduced into the chamber, and 10−20 W plasma is ignited. After the growth, the graphene on metal is cooled to room temperature under flowing gas, maintained at a constant pressure of 6 Pa. For growth conditions of different graphenes, refer to the Supporting Information.

Transfer of Graphene. After growth, graphene/alloy/sapphire is spin-coated with 800 nm of poly(methyl methacrylate) (PMMA, 996k MW, 8 wt % in anisole, 2000 rpm for 1 min) to facilitate wet transfer of the graphene film from the Cu/Ni alloy substrate. The etchant used is a 0.1 M ammonium persulfate ($(NH_4)_2S_2O_8$) aqueous solution. After twice etching, the PMMA/graphene is cleaned in DI water. Then, the floating PMMA/graphene is dried in the glovebox, then placed on the target SiO_2/Si substrate with the prepatterned array wells. Finally, the samples are gently transferred to a quartz tube furnace in order to remove the PMMA by annealing at 350 °C for more than 2 h with Ar and H_2 flow.

Fabrication of Prepatterned Holes. The array of holes on SiO_2/Si is produced by a standard micro/nanofabrication process. The Si

DOI: 10.1021/acsnano.8b00869
ACS Nano 2018, 12, 4529−4535

wafer with 285 nm oxide is first pattered by deep-UV photolithography, followed by a deep reactive ion etching to a 300 nm depth to form holes consisting of an 8 × 8 mm array of holes with 1.8 and 2.5 μm diameters.

Characterizations. The X-ray diffraction (XRD) is collected by a high-resolution Bruker D8-Discover diffractometer operating at 40 kV and 40 mA with Cu Kα radiation. Raman spectra are performed using a Witec/alpha 300 R confocal microscope with a 532 nm laser at ambient conditions. The SAED patterns and low-magnification TEM images are taken at 200 kV on a FEI F20, and the atomic resolution images were recorded using a FEI Titan G260-300 probe aberration-corrected scanning TEM with monochromator, which was operated at 80 kV to minimize knock-on damage.

AFM Nanoindentation. Indentation measurements are conducted in a Bruker AXS Dimension Icon AFM under atmospheric conditions with a 50 nm/s displacement rate toward the sample surface. The tip is a custom-fabricated diamond probe with a radius of 13.9 nm for mechanical testing. The spring constant calibration of the cantilever is accomplished by a combination of the thermal noise method and the Sader method, and a series of force spectroscopy measurements of CVD-grown single-crystal graphene is performed. Subsequently, the same probe is used to measure the nanocrystalline graphene films by indenting the center of the circle. A dozen holes are tested, and three to four force−displacement curves on each hole are measured by applying various maximum forces (0.2−1.5 μN) for each type of graphene film, respectively. Subsequently, the nanocrystalline graphene samples' deflection is acquired by subtracting the tip deflection based on the photodiode from the *z*-piezo displacement. Finally, 20−30 values for each type of graphene flake are independently recorded. Furthermore, in order to acquire the breaking toughness for different samples, the films are then indented with the same displacement rate until a membrane breaking event occurs.

ASSOCIATED CONTENT

Supporting Information

The Supporting Information is available free of charge on the ACS Publications website at DOI: 10.1021/acsnano.8b00869.

Methods and additional figures (PDF)

AUTHOR INFORMATION

Corresponding Author

*E-mail (L. B. Gao): lbgao@nju.edu.cn.

ORCID

Jiangwei Wang: 0000-0003-1191-0782

Libo Gao: 0000-0002-7822-9812

Notes

The authors declare no competing financial interest.

ACKNOWLEDGMENTS

This work was supported by the National Natural Science Foundation of China (Nos. 11674154 and 1171101156) and the Fundamental Research Funds for the Central Universities (Nos. 020414380036 and 020414380065).

REFERENCES

(1) Lee, C.; Wei, X.; Kysar, J. W.; Hone, J. Measurement of the Elastic Properties and Intrinsic Strength of Monolayer Graphene. *Science* **2008**, *321*, 385−388.

(2) Ruiz-Vargas, C. S.; Zhuang, H. L.; Huang, P. Y.; van der Zande, A. M.; Garg, S.; McEuen, P. L.; Muller, D. A.; Hennig, R. G.; Park, J. Softened Elastic Response and Unzipping in Chemical Vapor Deposition Graphene Membranes. *Nano Lett.* **2011**, *11*, 2259−2263.

(3) Huang, P. Y.; Ruiz-Vargas, C. S.; van der Zande, A. M.; Whitney, W. S.; Levendorf, M. P.; Kevek, J. W.; Garg, S.; Alden, J. S.; Hustedt, C. J.; Zhu, Y.; Park, J.; McEuen, P. L.; Muller, D. A. Grains and Grain Boundaries in Single-layer Graphene Atomic Patchwork Quilts. *Nature* **2011**, *469*, 389−392.

(4) Lopez-Polin, G.; Gomez-Navarro, C.; Parente, V.; Guinea, F.; Katsnelson, M. I.; Perez-Murano, F.; Gomez-Herrero, J. Increasing the Elastic Modulus of Graphene by Controlled Defect Creation. *Nat. Phys.* **2015**, *11*, 26−31.

(5) Zandiatashbar, A.; Lee, G.-H.; An, S. J.; Lee, S.; Mathew, N.; Terrones, M.; Hayashi, T.; Picu, C. R.; Hone, J.; Koratkar, N. Effect of Defects on the Intrinsic Strength and Stiffness of Graphene. *Nat. Commun.* **2014**, *5*, 3186.

(6) Liu, K.; Hsin, C.-L.; Fu, D.; Suh, J.; Tongay, S.; Chen, M.; Sun, Y.; Yan, A.; Park, J.; Yu, K. M.; Guo, W.; Zettl, A.; Zheng, H.; Chrzan, D. C.; Wu, J. Self-Passivation of Defects: Effects of High-Energy Particle Irradiation on the Elastic Modulus of Multilayer Graphene. *Adv. Mater.* **2015**, *27*, 6841−6847.

(7) López-Polín, G.; Gómez-Herrero, J.; Gómez-Navarro, C. Confining Crack Propagation in Defective Graphene. *Nano Lett.* **2015**, *15*, 2050−2054.

(8) Duong, D. L.; Han, G. H.; Lee, S. M.; Gunes, F.; Kim, E. S.; Kim, S. T.; Kim, H.; Ta, Q. H.; So, K. P.; Yoon, S. J.; Chae, S. J.; Jo, Y. W.; Park, M. H.; Chae, S. H.; Lim, S. C.; Choi, J. Y.; Lee, Y. H. Probing Graphene Grain Boundaries with Optical Microscopy. *Nature* **2012**, *490*, 235−239.

(9) Yazyev, O. V.; Chen, Y. P. Polycrystalline Graphene and Other Two-Dimensional Materials. *Nat. Nanotechnol.* **2014**, *9*, 755−767.

(10) Grantab, R.; Shenoy, V. B.; Ruoff, R. S. Anomalous Strength Characteristics of Tilt Grain Boundaries in Graphene. *Science* **2010**, *330*, 946−948.

(11) Rasool, H. I.; Ophus, C.; Klug, W. S.; Zettl, A.; Gimzewski, J. K. Measurement of the Intrinsic Strength of Crystalline and Polycrystalline Graphene. *Nat. Commun.* **2013**, *4*, 2811.

(12) Shekhawat, A.; Ritchie, R. O. Toughness and Strength of Nanocrystalline Graphene. *Nat. Commun.* **2016**, *7*, 10546.

(13) Sha, Z. D.; Wan, Q.; Pei, Q. X.; Quek, S. S.; Liu, Z. S.; Zhang, Y. W.; Shenoy, V. B. On the Failure Load and Mechanism of Polycrystalline Graphene by Nanoindentation. *Sci. Rep.* **2014**, *4*, e7437.

(14) Ma, T.; Liu, Z.; Wen, J.; Gao, Y.; Ren, X.; Chen, H.; Jin, C.; Ma, X.-L.; Xu, N.; Cheng, H.-M.; Ren, W. Tailoring the Thermal and Electrical Transport Properties of Graphene Films by Grain Size Engineering. *Nat. Commun.* **2017**, *8*, 14486.

(15) Gao, L.; Xu, H.; Li, L.; Yang, Y.; Fu, Q.; Bao, X.; Loh, K. P. Heteroepitaxial Growth of Wafer Scale Highly Oriented Graphene using Inductively Coupled Plasma Chemical Vapor Deposition. *2D Mater.* **2016**, *3*, 021001.

(16) Bae, S.; Kim, H.; Lee, Y.; Xu, X.; Park, J.-S.; Zheng, Y.; Balakrishnan, J.; Lei, T.; Ri Kim, H.; Song, Y. I.; Kim, Y.-J.; Kim, K. S.; Ozyilmaz, B.; Ahn, J.-H.; Hong, B. H.; Iijima, S. Roll-to-Roll Production of 30-inch Graphene Films for Transparent Electrodes. *Nat. Nanotechnol.* **2010**, *5*, 574−578.

(17) Thomson, J. J., XXIV. On the Structure of the Atom: An Investigation of the Stability and Periods of Oscillation of A Number of Corpuscles Arranged at Equal Intervals Around the Circumference of A Circle; with Application of the Results to the Theory of Atomic Structure. *Philos. Mag.* **1904**, *7*, 237−265.

(18) Li, N.-N.; Sha, Z.-D.; Pei, Q.-X.; Zhang, Y.-W. Hydrogenated Grain Boundaries Control the Strength and Ductility of Polycrystalline Graphene. *J. Phys. Chem. C* **2014**, *118*, 13769−13774.

(19) Lee, G.-H.; Cooper, R. C.; An, S. J.; Lee, S.; van der Zande, A.; Petrone, N.; Hammerberg, A. G.; Lee, C.; Crawford, B.; Oliver, W.; Kysar, J. W.; Hone, J. High-Strength Chemical-Vapor−Deposited Graphene and Grain Boundaries. *Science* **2013**, *340*, 1073−1076.

(20) Liu, K.; Wu, J. Mechanical Properties of Two-dimensional Materials and Heterostructures. *J. Mater. Res.* **2016**, *31*, 832−844.

(21) Lopez-Polin, G.; Jaafar, M.; Guinea, F.; Roldan, R.; Gomez-Navarro, C.; Gomez-Herrero, J. The Influence of Strain on the Elastic Constants of Graphene. *Carbon* **2017**, *124*, 42−48.

(22) Sha, Z. D.; Quek, S. S.; Pei, Q. X.; Liu, Z. S.; Wang, T. J.; Shenoy, V. B.; Zhang, Y. W. Inverse Pseudo Hall-Petch Relation in Polycrystalline Graphene. *Sci. Rep.* **2014**, *4*, 5991.
(23) Song, Z.; Artyukhov, V. I.; Yakobson, B. I.; Xu, Z. Pseudo Hall–Petch Strength Reduction in Polycrystalline Graphene. *Nano Lett.* **2013**, *13*, 1829–1833.
(24) Sen, D.; Novoselov, K. S.; Reis, P. M.; Buehler, M. J. Tearing Graphene Sheets From Adhesive Substrates Produces Tapered Nanoribbons. *Small* **2010**, *6*, 1108–1116.
(25) Kim, K.; Artyukhov, V. I.; Regan, W.; Liu, Y.; Crommie, M. F.; Yakobson, B. I.; Zettl, A. Ripping Graphene: Preferred Directions. *Nano Lett.* **2012**, *12*, 293–297.

DOI: 10.1021/acsnano.8b00869
ACS Nano 2018, 12, 4529–4535